Journal of Alloys and Compounds, 195 (1993) 419–426
JALCOM 7497

Vibrating Reed Studies of Vortex Pinning in High Temperature Superconductors

A. Gupta*, Y. Kopelevich†, P. Esquinazi, F.I. Schulz and H.F. Braun

Physikalisches Institut, Universität Bayreuth, P.O.Box 101251, W-8580 Bayreuth, Federal Republic of Germany

Abstract

The vibrating reed method has been used to study the dissipation due to vortex motion and the elastic coupling between vortices and pinning sites in single crystals of highly anisotropic superconductors. The results were obtained on small crystals of $Bi_2Sr_2CaCu_2O_{8+x}$ (T_c = 90.5 K), Y(6%Gd)$Ba_2Cu_3O_{6.83}$ (T_c = 67 K) and the organic superconductor κ-(BEDT-TT)$_2$Cu(NCS)$_2$ (T_c = 9.5 K) attached in different arrangements to a dielectric reed vibrating in a static magnetic field. The angle θ between the superconducting planes and the field direction could be varied from parallel to perpendicular orientation. For all these anisotropic quasi-2D materials, we observe two dissipation peaks as a function of temperature when $0° < \theta < 90°$ for all values of field. We show that the "depinning lines" defined by the peak position correspond to two flux diffusion modes within the model of thermally activated flux diffusion. They can be rescaled by $B \sin\theta$ to coincide with two constant resistivity lines.

1 Introduction

The vibrating reed technique has proved to be a powerful technique for the study of pinning and dissipation mechanisms in type II superconductors [1–5]. It has been successfully used to determine the "irreversibility" or "depinning" line (DL) in the magnetic field - temperature ($B-T$) plane of high temperature superconductors (HTS) [4–8].

In this paper we present systematic measurements of damping and resonance frequency enhancement for high temperature $Bi_2Sr_2CaCu_2O_{8+x}$ and Y(6%Gd)-$Ba_2Cu_3O_{6.83}$ and low temperature organic κ-(BEDT-TT)$_2$Cu(NCS)$_2$ superconducting single crystals performing tilt vibrations in an applied magnetic field B. Different vibration configurations and field orientations with respect to the conducting planes have been used to probe the $B-T$ plane.

In section 3, we discuss theoretically and experimentally the resonance frequency enhancement as a function of magnetic field for a superconducting slab performing tilt oscillations in different configurations.

Based on the model of thermally activated flux flow (TAFF) [6–11], we discuss in section 4 the appearance of two dissipation peaks [12–14], taking into account the layered nature of these vibrating quasi-2D superconductors. We show that the angular scaling of the characteristic peak temperature in an applied field B inclined by an angle $0° < \theta < 90°$ with respect to the conducting planes resembles the scaling of resistivity observed in these materials [15–17].

Finally, we compare the activation barriers as determined from the published resistivity data of different Bi-based, oxygen-deficient and fully oxygenated Y-based and organic superconductors in section 5. We show that in the layered organic superconductors, in spite of their much lower critical temperatures, the vortex motion is diffusive in character [12] due to a relatively small ratio U_b/kT_c, where U_b is the effective activation barrier for vortex motion, comparable to those of Bi-based and oxygen deficient Y-based high temperature superconductors.

2 Experimental and sample details

The resonance frequency enhancement $\Delta\nu = \nu(B,T) - \nu(0,T)$ and excess damping $\Gamma = \Gamma(B,T) - \Gamma(0,T)$ of small superconducting single crystals attached to a vibrating reed were measured both isothermally as a function of magnetic field B and as a function of temperature T at fixed field in a broad field regime of 0.01 T – 8 T. In all measurements a small crystal was glued with vacuum grease to a host reed, fabricated from polymer resin or MgO with typical reed dimensions between $L \times w \times d = 8 - 12 \times 1 - 2 \times 0.1 - 0.2$ mm^3 with a gold layer (typically $\simeq$ 40 nm) sputtered on both surfaces. Without the crystal, there was no significant magnetic field dependence from the host reed.

We use three configurations, designated CONF1, CONF2 and CONF3 (Fig. 1), in which the supercon-

*present address: DPMC, Université de Genève, Quai Ernest-Ansermet 24, CH-1211 Genève 4
†permanent address: A. F. Ioffe Physical-Technical Institute, St. Petersburg, Russia

0925-8388/93/$06.00

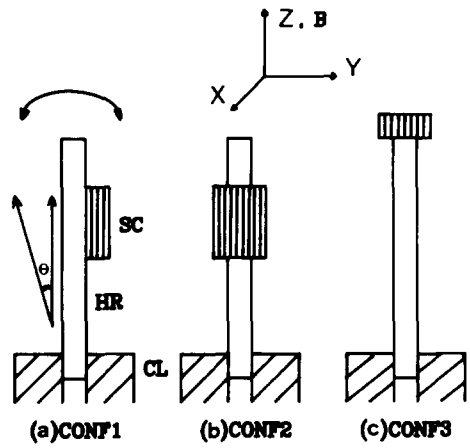

Fig. 1. Schematic of the nonconducting reed with an attached small superconducting crystal platelet in three configurations (a) CONF1, (b) CONF2, (c) CONF3. θ represents the angle between applied field B and superconducting planes. CL: Clamp, HR: Host Reed (Nonconducting), SC: Superconducting crystal.

ducting single crystal platelet of length L_p , width w_p and thickness d_p ($L_p, w_p \gg d_p$, large face parallel to the conducting planes) is attached to the vibrating host reed. In CONF1 and CONF2, B is either parallel (CONF1 and CONF2) or perpendicular (CONF3) to the superconducting planes. The host reed vibrates in the z, y-plane which causes a tilt oscillation of the sample about the x-axis with a small angular amplitude ($\phi_0 \lesssim 10^{-5}$ rad).

Angle dependent measurements were performed in CONF1 (Fig. 1a), with the reed holder rotated about the x-axis by a fixed angle θ. Note that θ represents the angle between the conducting planes and the applied field, with the reed at rest. The experimental setup for vibrating reed measurements has been described in detail in Ref. [2].

Results on superconducting single crystals of $Bi_2Sr_2CaCu_2O_{8+x}$ (BSC1: $2 \times 0.9 \times 0.02$ mm^3, BSC2: $1.8 \times 1 \times 0.025$ mm^3), Y(6%Gd)$Ba_2Cu_3O_{6.83}$ (YGBC1: $1.7 \times 0.25 \times 0.025$ mm^3) and organic κ-(BEDT-TT)$_2$Cu(NCS)$_2$ (KORG1: $1 \times 0.6 \times 0.02$ mm^3) are presented. The single crystals used in this work were optically clean and for the Bi- and Y-crystals, the stoichiometry mentioned was confirmed by microprobe analysis.

Details on crystal preparation and characterization have been published elsewhere [18–20]. Their transition temperature T_c, determined from the onset of excess dissipation using the vibrating reed in CONF1 with $\theta \simeq 0°$ and measured with $B \leq 0.1$ T are 90.5 K for both BSC1 and BSC2, 67 K for YGSC1 and 9.5 K for KORG1.

3 Frequency enhancement as a function of magnetic field

3.1 Theory

We consider an applied magnetic field $B \gg B_{c1}$, such that the static magnetization can be neglected and the applied field is nearly equal to the field inside the superconducting platelet. In general, the resonance frequency of a vibrating superconductor in a magnetic field increases as a result of an extra magnetic line tension pulling along the reed [1, 3]. Depending on the geometry of the reed arrangement, this extra line tension can be attributed to surface shielding currents, FLL tilt modulus and elastic pinning force between the FLL and pinning sites (for details see [1–5]). Below we give expressions for the line tension appropriate for the different configurations shown in Fig. 1.

In CONF1 (Fig. 1a), if $L_p \gg (\pi w_p/4d_p)\lambda_{44}$, where $\lambda_{44} = (C_{44}/\alpha)^{1/2}$ is the tilt penetration depth [1], $C_{44} \simeq B^2/\mu_0$ the FLL tilt modulus, and α the Labusch parameter, the line tension P_1 arises from the surface currents generated on the main surface of the crystal due to the shielding of the small ac field component created when the reed tilts by a small angle ϕ in the magnetic field. P_1 will be given by the same expression as derived for a bulk superconducting reed in [1], except that it will be reduced by a geometrical factor $w_p^2 L_p/w^2 L$, $P_1 = \pi(w_p/2)^2 B^2 L_p/L\mu_0$.

A second, smaller contribution due to the tilt modulus of the FLL becomes important in CONF2 (Fig. 1b), where the shielding contribution can be neglected. If $L_p/2 \gg \lambda_{44}$, the line tension is $P_2 = w_p d_p B^2 L_p/L\mu_0$. If $L_p/2 \leq \lambda_{44}$, then the line tension will be proportional to the elastic coupling constant α between the FLL and pinning centers, $P_3 \approx wdf\alpha g$. Here, f corresponds to the volume ratio of platelet and host reed, and g is a geometrical factor which depends on the shape of the platelet. For a parallelepiped platelet in CONF2 $g = L_p^2/3$.

The line tension in the configuration CONF3 (Fig. 1c) will have an origin similar to that of CONF2, except that the relevant dimension to be compared with λ_{44} is now d_p, thus $g = d_p^2/3$.

For a volume ratio of the crystal to the host reed $f \ll 1$, we can approximately represent the frequency enhancement in the three configurations by the following relation:

$$\Delta\omega^2 = \omega^2(B) - \omega^2(0) \approx 4.65 P_i/(\rho_h dw L^2) \qquad (1)$$

where P_i is the line tension relevant for a particular configuration i, $\omega = 2\pi\nu$, and ρ_h is the density of the host reed.

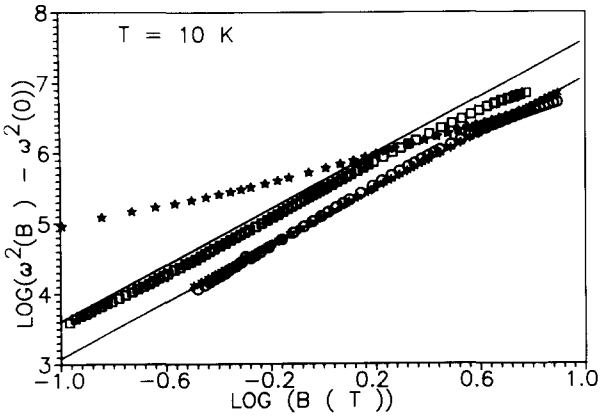

Fig. 2. Resonance frequency enhancement as a function of magnetic field at a fixed temperature of 10 K for single crystals Y(6%Gd)$Ba_2Cu_3O_{6.83}$: (*) CONF1, (O) CONF3 and $Bi_2Sr_2CaCu_2O_{8+x}$(BSC1): (□) CONF1, (★) CONF3. The solid lines represent the frequency enhancement calculated using eq. 1.

3.2 Experimental Results

The measured enhancement of the (squared) resonance frequency $\Delta\omega^2$ as a function of applied magnetic field B at a fixed temperature for both the YGBC1 and BSC1 crystals is depicted in Fig. 2.

For the YGBC1 crystal we estimate $\lambda_{44} = (C_{44}/\alpha)^{1/2} = 32$ μm at 20 K and $B = 1$ T. (The value of α was taken from the measurements on the same crystal for $B \parallel CuO_2$ planes [21]). In CONF1, the condition $\lambda_{44} = 32$ μm $\ll L_p/2 = 0.85$ mm is easily fulfilled and indeed the observed $\omega^2(B) - \omega^2(0) \propto B^2 \propto C_{44} \propto P_2$. In CONF3 ($B \perp CuO_2$ planes) almost the same magnitude of frequency enhancement $\Delta\omega^2 \propto B^2$ as in CONF1 is observed (Fig. 2). This indicates a tilt modulus contribution to frequency enhancement in CONF3. Using eq. 1 and the correct line tension P_i for CONF1 and CONF3, we can fit the frequency enhancement as a function of field for both configurations (solid line in Fig. 2). However, since $d_p/2 = 12.5$ μm for the YGBC1 crystal, this result implies $\lambda_{44}(B \perp CuO_2$ planes$) < \lambda_{44}(B \parallel CuO_2$ planes$) = 32$ μm. This is possible, as λ_{44} in anisotropic superconducting crystals can be different for different direction of fields and is determined by the value of α in that direction. A deviation from a B^2 behavior results at high fields when (Fig. 2) thermally activated depinning becomes important.

For the BSC1 crystal in CONF2 ($B \parallel CuO_2$ planes) we again find $\Delta\omega^2 \propto B^2$. In contrast, in CONF3 ($B \perp CuO_2$ planes), the frequency enhancement shows an almost linear behavior with field (Fig. 2). This B dependence in CONF3 certainly indicates that the line tension is now not dominated by C_{44} any more, rather it should be proportional to α. Using the known dimensions of the crystal and the expression for P_3 in eq. 1, we obtain for $T = 10$ K and $B = 1$ T $\alpha = 1.6 \times 10^{15}$ N/m^4 and $\lambda_{44} = 22$ μm. This value of λ_{44} is much smaller than the 130 μm obtained for a Bi-based polycrystalline system [3]. However, $d_p/2 = 10$ μm $< \lambda_{44} = 22$ μm $\ll L_p/2 = 1$ mm, which is in good agreement with the observed variation of $\Delta\omega^2 \propto B^2 \propto C_{44} \propto P_2$ for CONF2 (see also below) and $\Delta\omega^2 \propto \alpha(B)$ for CONF3.

For the BSC1 crystal in CONF2, according to the model of Kes et al. [15], the magnetic field should penetrate the space between CuO_2 planes without forming an Abrikosov lattice. Interestingly, our measurements in this configuration for the BSC1 crystal show a large frequency enhancement $\propto B^2$. The contribution related with Abrikosov vortices generated perpendicular to the CuO_2 planes by a misalignment angle between applied field and CuO_2 planes in CONF2, estimated to be $\lesssim 3°$, would be far too small ($\lesssim B^2 \sin^2 3°$) to produce the observed large frequency enhancement. Further, the surface currents in the x, z-plane are negligible because of the extremely small crystal thickness. The frequency enhancement can only be understood with a C_{44} contribution coming from the field penetrating the intraplanar region. Assuming that these FLs $\parallel CuO_2$ planes are pinned and contribute to the frequency enhancement, we get a good agreement between the results of CONF2 and the frequency enhancement calculated using eq. 1 and line tension P_2 (solid line in Fig. 2). The discrepancy seen between the theoretical line and the experimental points can be understood assuming weak pinning in Bi-2212.

4 Thermally activated depinning

4.1 Theory

Let us consider a perfectly rectangular crystal platelet aligned as shown in Fig. 3, oscillating about the x-axis with angular amplitude ϕ_0 in a magnetic field B inclined at an arbitrary angle $0° < \theta < 90°$ in the y, z-plane. Due to the periodic oscillations, an *ac* field component is generated perpendicular to the sets of parallel faces A, C, with amplitude $b_A, b_C \lesssim 1$ μT $\ll B$ and frequency ω, the resonance frequency of the vibrating reed. If the third crystal face is not aligned perpendicular to the rotation axis, an *ac* field b_B normal to it will be present.

Within the model of thermally activated flux flow (TAFF), the penetration of the *ac* field into the crystal is governed by FLL diffusion with a diffusivity

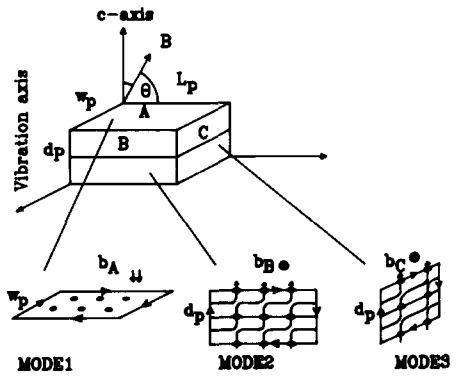

Fig. 3. Upper part: A vibrating superconducting slab, with magnetic field oriented at an arbitrary angle θ with respect to the conducting planes. Lower part: Three possible diffusion modes as viewed from the three faces of the slab with point vortices of density $B\sin\theta$ along with the ac field components of magnitude b_A, b_B, b_C. The arrows on the edges indicate the flow of currents generated by the ac field components.

$D = \rho/\mu_0$ which in an anisotropic medium will depend on the direction of the flux motion. For small driving forces, the high temperature superconductors show a linear resistivity in a broad temperature regime below T_c due to thermally activated flux flow

$$\rho(B,T,\theta) = \rho_{FF}\exp\left(-U_b(B,T,\theta)/kT_c\right) \qquad (2)$$

where ρ_{FF} is the flux flow resistivity and U_b is an effective activation barrier for vortex motion. The limit of current-independent activation applies to the present vibrating reed experiments, as has been verified by the independence of the reed response on oscillation amplitude [22].

In the general case discussed above, we have three diffusion modes, which give rise to three different skin depths δ for the three main platelet dimensions.

$$\delta_i^2 = 2D_i/\omega = 2\rho_i(B,T,\theta)/(\mu_0\omega) \qquad (3)$$

At fixed B and θ, the skin depth increases with $D_i(B,T,\theta)$ at increasing temperature. At some characteristic value of $D_i(B,T_{Di},\theta)$, at the so-called depinning temperature T_{Di}, δ_i becomes equal to the relevant dimension l_i of the crystal, different for each mode, and a peak in dissipation accompanied with a step in frequency enhancement is observed. At a fixed angle, each mode gives rise to a depinning line (DL) as a function of applied field $T_{Di}(B,\theta)$ which is equivalent to a line of constant resistivity for

$$\rho_i(B,T_{Di},\theta) \simeq \omega l_i^2/\pi^2 \qquad (4)$$

If the relevant dimension for each mode is known, then the measured DL can be compared with the corresponding constant resistivity line.

We now discuss the relevant resistivity and dimension in each mode for highly anisotropic Bi-2212. According to Kes et al. [15], in a field B inclined an angle θ with respect to the CuO_2 planes, the perpendicular component penetrates in form of point vortices with a density $B\sin\theta$, and the field component parallel to the planes penetrates the crystal without forming vortices.

In MODE1, the currents due to the probing field generate a compression on the point vortices, which diffuses along the width or length of the crystal (see Fig. 3). The relevant resistivity is the in-plane resistivity ρ^c_{ab} (upper indices characterize the field direction, lower indices the current direction) due to the point vortices. The damping peak is due to the ac field penetration along the smaller dimension, the width w_p, since once the field has entered along w_p, it need no longer penetrate along L_p.

In MODE3, the currents along the thickness are in a force free configuration with respect to the point vortices, whereas the currents along the width of the crystal generate a "tilt" of the point vortices, which penetrates the crystal along the thickness d_p (see Fig. 3). In MODE2, present if $b_B \neq 0$, the situation is just as in MODE3, with the role of length and width interchanged. In both cases, the relevant resistivity is again the in-plane resistivity ρ^c_{ab}. Since MODE2 and MODE3 are equivalent, they will not give rise to separate dissipation peaks, and at any arbitrary angle $0° < \theta < 90°$ only two peaks in dissipation will be observed. The penetration of the ac field in all the modes in a Bi-2212 crystal will thus be governed by the motion of the point vortices due to the $B\sin\theta$ component and only the linear in-plane resistivity ρ^c_{ab} data is required for comparison with a DL. Indeed, the resitivity ρ^θ_{ab} in these layered quasi-2D compounds scales with $B\sin\theta$ [16,17],

$$\rho^\theta_{ab}(B,T,\theta) = \rho^c_{ab}(B\sin\theta,T). \qquad (5)$$

Thus, for all modes the depinning lines $T_{Di}(B,\theta)$ should scale with $B\sin\theta$. We would like to mention here that the frequency enhancement in these modes at temperatures less than T_{Di} can have different contributions, as shown in section 3.

In the light of the recent observation [23,24] of much higher Arrhenius resistivity ρ^c_c, i.e. when the field is applied along the c-axis and the measuring current flows along the c-axis in a force free configuration, the faster diffusion could occur along L_p in MODE2 and along w_p in MODE3 (see Fig. 3) in thicker crystals instead of along d_p. Note that both these modes are not equivalent due to different dimensions involved and one expects then three dissipation peaks. Since

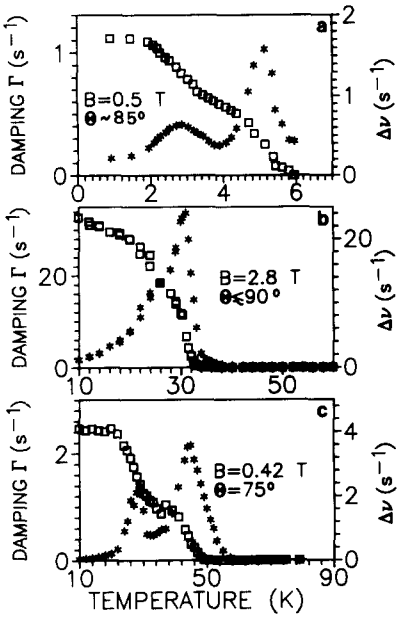

Fig. 4. Damping and resonance frequency enhancement as a function of temperature in the single cyrstals of (a) κ-(BEDT-TT)$_2$Cu(NCS)$_2$ in CONF3, (b) Y(6%Gd)Ba$_2$Cu$_3$O$_{6.83}$ in CONF3 and (c) Bi$_2$Sr$_2$CaCu$_2$O$_{8+x}$ in CONF1. Measurements in CONF3 with slightly misaligned crystal $90° > \theta \gtrsim 85°$.

the dissipation mechanism for this configuration is not clear at present, we postpone a further empirical discussion to the experimental section 4.2.

4.2 Experimental Results

In Fig. 4 we show damping peaks and frequency enhancement as a function of temperature in an applied field B for all three compounds. In every case, a double peak structure of the damping accompanied with respective changes of resonance frequency is observed. As discussed, this behavior indicates the presence of two diffusion modes, corresponding to two different length scales w_p (MODE1, high temperature peak) and d_p (MODE3, low temperature peak) for the penetration of the *ac* field. Note that the measurements for YGSC1 and KORG1 presented in Fig. 4 were performed in CONF3, with the conducting planes not exactly aligned $\perp B$, i.e. $90° \neq \theta \gtrsim 85°$. In the following, we discuss the depinning lines obtained by such measurements at different fields and angles for each of these compounds separately.

We now show for each mode the scaling of the DL with the $B_i = B\sin\theta$ component measured for the BSC2 crystal. The temperatures corresponding to both damping peaks (see Fig. 4) obtained in the angular measurements in CONF1 are plotted as a function of field component perpendicular to CuO_2 planes $B\sin\theta$ in Fig. 5. We observe that for each mode the reduced depinning temperatures T_D/T_c at different angles coalesce perfectly on a single DL. Similar scaling has been also reported in [14, 25, 22] using both vibrating reed and *ac* susceptibility measurements on a Bi-2212 crystal. As discussed in section 4.1 within the diffusion picture, these two DLs should match the constant resistivity lines. Taking the resonance frequency of the reed $\nu = 1.0$ kHz and using eq. 4 with the relevant l_i for both modes, we get for the lower and upper DL constant ρ criteria of $6 \times 10^{-5}\mu\Omega$cm and $9.6 \times 10^{-2}\mu\Omega$cm, respectively. In the same figure we compare these DLs with the respective constant in-plane resistivity lines taken from [26]. The matching of both the DLs with constant ρ lines is remarkable and establishes their origin in finite resistivity due to diffusive FLL motion.

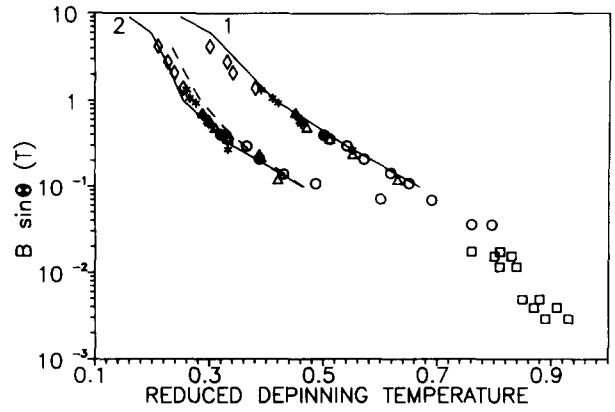

Fig. 5. Reduced depinning temperatures of the single crystal Bi$_2$Sr$_2$CaCu$_2$O$_{8+x}$ (BSC2) in CONF1 as a function of field component $\perp$ CuO_2 planes, $B\sin\theta$ for both modes. (◇): 90°, (*): 75°, (△): 60°, (○): 45°, 30°, 15°, (□): 2.6°, 1.4°, 0.4°. The solid lines are constant resistivity $\rho^c_{a,b}$ lines corresponding to $\rho = 9.6 \times 10^{-2}\mu\Omega$cm (1) and $6 \times 10^{-5}\mu\Omega$cm (2) taken from [26]. The dashed line represents a constant resistivity $= 9.6 \times 10^{-2}\mu\Omega$cm line taken from ρ^c_c data of [24].

In view of our extrapolation of Arrhenius resistivity to lower temperatures, we would like to make three remarks regarding the recently observed non-Arrhenius linear resistivity at low temperatures [27]: (1) the upper constant resistivity line lies in the region where the resistivity behavior is still Arrhenius, (2) the lower constant resistivity line does not shift by more than 3% even if the non-Arrhenius behavior is taken into account, (3) even if at low temperatures the FLL is in a vortex glass state, the dissipation peaks can be well accounted for by diffusion modes.

As mentioned in section 4.1, if ρ^c_c would cause the

penetration of the probing *ac* field in both MODE2 and MODE3, then three damping peaks should be observable. In the geometry used in Fig. 1a there might be only a negligible *ac* field (b_B) on the crystal face in the y,z-plane and MODE2 probably cannot be observed. If we consider the low temperature peak due to MODE3 with a relevant dimension $l_3 = w_p$ and ρ_c^c as the relevant resistivity, the constant resistivity ρ_c^c line (see dashed line in Fig. 5), taken from [24] measured on a 87 K Bi-2212 crystal, also lies near the depinning line. Thus, to unambiguously determine the origin of MODE3, further measurements are needed on crystals with comparable width and thickness, or on a crystal rotated parallel to the CuO_2 planes on the host reed in CONF1.

The depinning temperatures T_{Di} corresponding to both the modes in the YGBC1 crystal are plotted in Fig. 6 as a function of $B\sin\theta$ for all measured angles. Similar to the Bi-based compounds, for this low oxygen content YGBC1 crystal again all the $T_{Di}(B,\theta)$ data collapse onto a single DL for each mode. Using the known resonance frequency of 0.65 kHz and the corresponding diffusion lengths d_p and w_p for the two modes, we obtain the constant resistivity criteria of 2.1×10^{-5} and $3.2\times10^{-2}\mu\Omega$cm, respectively. Constant in-plane resistivity lines (taken from [28]) measured for a low oxygen content Y-123 crystal are also shown in the same figure. The small mismatch of the DLs and constant ρ lines could be due to different oxygen concentration in the two crystals. Another explanation for the mismatch of the lower DL, which needs further investigation, might be that in MODE3, the relevant resistivity is ρ_c^c instead of $\rho_{a,b}^c$.

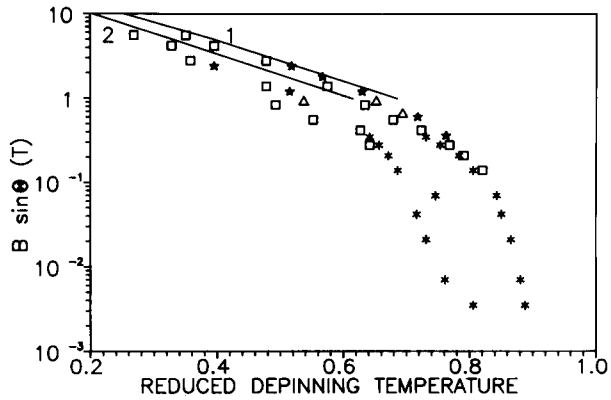

Fig. 6. Reduced depinning temperatures of the single crystal Y(6%Gd)$Ba_2Cu_3O_{6.83}$ in CONF1 as a function of field component $\perp$ CuO_2 planes, $B\sin\theta$, for both modes. (□): 90°, (★): 75°, (△): 60°, (*): 2.5°. The solid lines are constant resistivity $\rho_{a,b}^c$ lines corresponding to $\rho = 3.2\times10^{-3}\mu\Omega$cm (1) and $2.1\times10^{-5}\mu\Omega$cm (2) taken from [28].

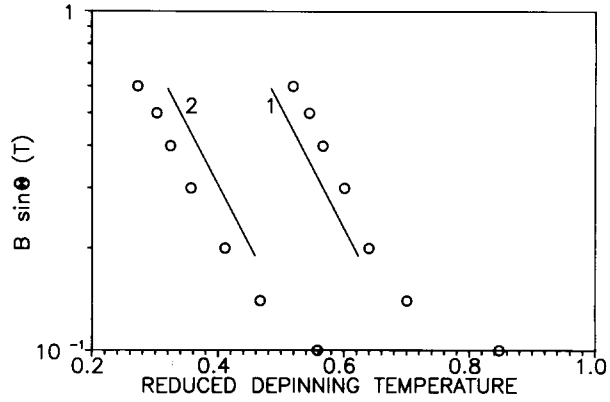

Fig. 7. Reduced depinning temperatures of the single crystal κ-(BEDT-TT)$_2$Cu(NCS)$_2$ as a function of field measured in CONF3 with $90° > \theta \gtrsim 85°$. The solid lines are constant resistivity $\rho_{a,b}^c$ lines corresponding to $\rho = 10^{-2}\mu\Omega$cm (1) and $10^{-5}\mu\Omega$cm (2) taken from [29].

The depinning lines measured on K-(BEDT-TT)$_2$-Cu(NCS)$_2$ related with two modes observed in CONF3 with $90° > \theta \gtrsim 85°$ are shown in Fig. 7. Using the known resonance frequency, the relevant dimensions w_p (MODE1) and d_p (MODE3) in eq. 4, we obtain constant resistivty criteria of $10^{-2}\mu\Omega$cm and $10^{-5}\mu\Omega$cm, respectively. The corresponding constant resistivity lines obtained from the extrapolation of the replotted in-plane resistivity data of [29] on a κ-(BEDT-TT)$_2$-Cu(N(CN)$_2$)Br crystal are also shown in Fig. 7. The resemblance is quite reasonable.

5 Activation barrier

In Fig. 8, we compare the reduced activation barriers as obtained from the slopes of Arrhenius plots of the resistivity data taken from literature for all three systems discussed above.

For Bi-2212, the in-plane resistivity data ρ_{ab}^c of three different crystals measured in [24,26,30], and ρ_c^c data of [24] have been used. Two results can be noted. Firstly, within a 10% error of the extrapolation, the value of the activation barrier is the same for all the crystals in spite of their different T_c's. This could indicate that the activation barrier is not so sensitive to the oxygen content in the Bi-2212 system as in the Y-123 system. Secondly, the activation barrier is independent of the direction of the current with respect to the point vortices in Bi-2212 (see also [23]).

For κ-(BEDT-TT)$_2$Cu(NCS)$_2$, there are two important observations. The reduced activation barriers U_b/kT_c are of same order of magnitude as for Bi-2212 and oxygen-deficient Y-123 compounds, which lends

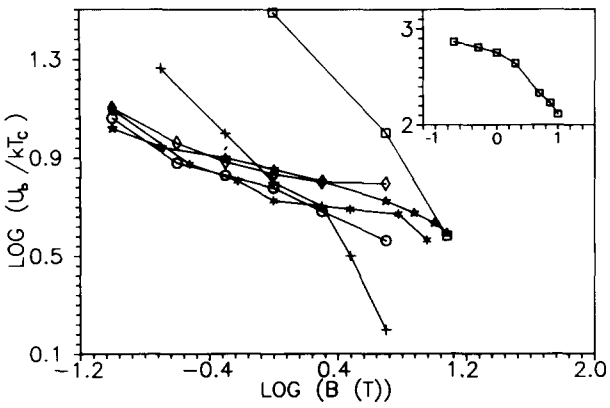

Fig. 8. Reduced activation barrier as a function of applied magnetic field ⊥ CuO_2 planes on a double logarithmic scale, calculated from the slope of the Arrhenius plots of the resistivity taken from literature. $Bi_2Sr_2CaCu_2O_{8+x}$: Activation barrier from $\rho^c_{a,b}$ data of [30] (★), [26] (*), [24] (○); ρ^c_c data of [24] (◇). Oxygen deficient Y(6%Gd)$Ba_2Cu_3O_{6.83}$: $\rho^c_{a,b}$ data of [28] (□). κ-(BEDT-TT)$_2$Cu(NCS)$_2$: $\rho^c_{a,b}$ data of [29] (+). Inset: Similar plot for fully oxygenated $YBa_2Cu_3O_7$: $\rho^c_{a,b}$ data of [28] (□).

credibility to an interpretation in terms of diffusive FLL motion even at low temperatures. The field dependence of the activation barrier resembles that of oxygen deficient Y-123. It should be noted, that the Arrhenius plot of resistivity for each value of magnetic field is valid in a limited temperature range (see the literature cited).

6 Conclusions

In this work we have given a qualitative description of the origin of resonance frequency enhancement in a vibrating combination of a host reed with an attached superconducting crystal. Depending on the pinning strength α, dimensions of the crystal and the orientation of magnetic field, the origin of restoring force can be shielding field energy, the tilt modulus C_{44} or the Labusch parameter α itself. CONF2 turns out to be an interesting geometry to study the properties of FLs aligned parallel to the conducting planes in layered superconductors. In this configuration, our results indicate a substantial frequency enhancement in Bi-2212 compound.

For angles $0° < \theta < 90°$ we observe two peaks in damping for all three compounds Bi-2212, oxygen deficient Y-123 and κ-(BEDT-TT)$_2$Cu(NCS)$_2$, resulting from two diffusion modes of flux penetration. The damping peak temperatures corresponding to each mode scale with $B \sin\theta$. The rescaled DLs collapse on a single curve and match the constant in-plane resistivity lines, consistent with the TAFF model for all the three compounds. More work is needed to establish the role of ρ^c_c in the penetration of an *ac* field in these layered superconductors.

Acknowledgments

It is a pleasure to thank W. Ettig for his technical help. This work was supported by the DAAD (Y. K.) and the Bayerische Forschungsstiftung under FORSUPRA.

References

1 E. H. Brandt, P. Esquinazi and H. Neckel, J. Low Temp. Phys. **63** (1986) 187.
2 P. Esquinazi, H. Neckel, G. Weiss and E. H. Brandt, J. Low Temp. Phys. **64** (1986) 1.
3 J. Kober, A. Gupta, P. Esquinazi, H. F. Braun and E. H. Brandt, Phys. Rev. Lett. **66** (1991) 2507.
4 P. Esquinazi, J. Low Temp. Phys. **85** (1991) 139.
5 A. Gupta, Ph. D. thesis, Univ. Bayreuth, 1991, unpublished.
6 P. H. Kes, J. van den Berg, C. J. van der Beek, and J. A. Mydosh, Supercond. Sci. Technol. **1** (1989) 242.
7 A. Gupta, P. Esquinazi, H. F. Braun and H.-W. Neumüller, Phys. Rev. Lett. **63** (1989) 1869.
8 A. Gupta, P. Esquinazi, H. F. Braun, W. Gerhäuser, H.-W. Neumüller, K. Heine and J. Tenbrink, Europhys. Lett. **10** (1989) 663.
9 P. Esquinazi, Solid State Comm. **74** (1990) 75.
10 E. H. Brandt, Z. Phys. B **80** (1990) 167.
11 E. H. Brandt, Int. J. Mod. Phys. B **5** (1991) 751.
12 Y. Kopelevich, A. Gupta, P.Esquinazi, C.-P. Heidmann and H. Müller, Physica C **183** (1991) 345.
13 E. H. Brandt, Phys. Rev. Lett. **68** (1992) 3769.
14 C. Durán, J. Yazyi, F. de la Cruz, D.Bishop, D. Mitzi and A. Kapitulnik, Phys. Rev. B **44**, (1991) 7737.
15 P. H. Kes, J. Aarts, V. M. Vinokur and C. J. van der Beek, Phys. Rev. Lett. **64** (1990) 1063.
16 Y. Iye, S. Nakamura and T. Tamegai, Physica C **174** (1991) 227.
17 H. Raffy, S. Labdi, O. Laborde and P. Monceau, Phys. Rev. Lett. **66** (1991) 2515.
18 F. I. Schulz, Diploma thesis, Univ. Bayreuth, 1991, unpublished.
19 D. Shaltiel, S. E. Barnes, H. Bill, M. Francois, H. Hagemann, J. Jegondaz, D. Lovy, P. Monod,

M. Peter, A. Revcolevschi, W. Sadowski and E. Walker, Physica C **161** (1988) 441.

20 H. Müller, C.-P. Heidmann, D. Kellner, W. Biberacher, and K. Andres, Proc. ICSM '90, Synthetic Met. **39** (1990) 261.

21 A. Gupta, P. Esquinazi, H. F. Braun, W. Sadowski, E. Walker and D. Shaltiel, Bull. Mater. Res. (Indian) **14** (1991) 877.

22 Y. Kopelevich, A. Gupta and P. Esquinazi, to be published.

23 Yu. I. Latyshev and A. F. Volkov, Physica C **182** (1991) 47.

24 R. Busch, G. Ries, H. Werthner, G. Kreiselmeyer, and G. Saemann-Ischenko, Phys. Rev. Lett. **69** (1992) 522.

25 J. Yazyi, A. Arribére, C. Durán, F. de la Cruz, D. Mitzi and A. Kapitulnik, Physica C **184** (1991) 254.

26 J. W. P. Hsu, D. B. Mitzi, A. Kapitulnik and M. Lee, Phys. Rev. Lett. **67** (1991) 2095.

27 H. Safar, P. L. Gammel, D. J. Bishop, D. B. Mitzi, and A. Kapitulnik, Phys. Rev. Lett. **68** (1992) 2672.

28 T. T. M. Palstra, B. Batlogg, R. B. van Dover, L. F. Schneemeyer and J. V. Waszczak, Phys. Rev. B. **41** (1990) 6621; T. T. M. Palstra, B. Batlogg, R. B. van Dover, L. F. Schneemeyer and J. V. Waszczak, Appl. Phys. Lett. **54** (1989) 763.

29 W. K. Kwok, U. Welp, K. D. Carlson, G. W. Crabtree, K. G. Vandervoot, H. H. Wang, A. M. Kini, J. M.Williams, D. L. Stupka, L. K. Montgomery and J. E. Thompson, Phys. Rev. B **42** (1990) 8686.

30 T. T. M. Palstra, B. Batlogg, L. F. Schneemeyer and J. V. Waszczak, Phys. Rev. Lett. **61** (1988) 1662.